Monthly Notices of the ROYAL ASTRONOMICAL SOCIETY

MNRAS **439,** 3790–3797 (2014) doi:10.1093/mnras/stu229
Advance Access publication 2014 February 28

Appearance of an accretion disc perturbed by fractional Brownian Motion density

G. Mocanu,[1,2]★ N. Magyar,[1] A. Pardi[1] and A. Marcu[1]★

[1]*Faculty of Physics, Babes-Bolyai University, No. 1 Kolgalniceanu Street, 400084 Cluj-Napoca, Romania*
[2]*Department of Mathematics, Technical University of Cluj Napoca, Memorandumului Street 28, 400114 Cluj-Napoca, Romania*

Accepted 2014 January 31. Received 2014 January 27; in original form 2013 May 3

ABSTRACT

This paper aims to investigate/map the effects that perturbations applied to an accretion disc might produce on the registered light curves (LCs). The case of accretion discs around supermassive active black holes (AGNs) is studied with the goal to explain some of the statistical properties of the observed intraday variability (IDV). The region producing optical IDV is perturbed by allowing it to develop a mass density of a fractional Brownian Motion-like type. The LCs and spectral slopes are calculated and compared to observational data for different Hurst parameters. The spectral slopes of the simulated LCs vary in the range (0.4, 2.5). The agreement with observational data shows that a magnetized disc subjected to stochastic perturbations can produce some of the features observed in the LCs.

Key words: accretion, accretion discs – MHD – radiation mechanisms: non-thermal – BL Lacertae objects: general – BL Lacertae objects: individual: S5 0714+714.

1 INTRODUCTION

Extensive observational and theoretical efforts have been made in order to explain intraday variability (IDV) in some classes of active galactic nuclei (AGNs) (Mineshige, Ouchi & Nishimori 1994; Wagner et al. 1996; Balbus & Hawley 1998; Krichbaum et al. 2002; Poon, Fan & Fu 2009). IDV manifests as the fast change (in less than one day) in the luminosity output of an object, and for supermassive black holes IDV occurs in the optical domain. The power spectral distribution (PSD) of these light curves (LCs) are found to be non-trivial (Azarnia, Webb & Pollock 2005; Carini, Walters & Hopper 2011; Leung et al. 2011). A large percentage of AGN evolve so as to produce IDV in the optical with PSD for which the spectral slope α is neither 0 nor -2, as shown by structure function analysis (Carini et al. 2011), fractal dimension analysis (Leung et al. 2011) and discrete Fourier transform analysis (Azarnia et al. 2005).

These types of analyses lead to the conclusion that the disc is perturbed by a stochastic noise; further discussion on this topic can be found in, e.g., MacLeod et al. (2010), who find no convincing case of periodicity in LCs for a 9000 quasar sample and state that these type of oscillations are entirely expected from coloured noise processes; Montagni et al. (2006) conclude, in a discussion of optical IDV in BL Lacs, that IDV is essentially a stochastic process; Dexter & Agol (2011) state that it is unlikely that the observed quasar variability is caused by a coherently varying accretion disc.

For BL Lac S5 0716+714, the spectral slope was found to vary from 1.083 to 2.65 for the IDV data set discussed in Mocanu & Marcu (2012) and Poon et al. (2009), from 0.6 to 2.22 for the data set discussed in Carini et al. (2011), from 0.8 to 1.4 in the data set discussed in Azarnia et al. (2005) and from 0.6 to 1.7 in the data set discussed in Leung et al. (2011).

We start from the assumption that the source of IDV is placed within a geometrically thin, optically thick disc. An equilibrium rotating accretion disc in the magnetohydrodynamic (MHD) framework is perturbed (Section 3) by a fractional Brownian Motion (fBM) process in density. The MHD equations are solved to obtain the perturbed variables needed to compute the Reynolds–Maxwell stress tensor component responsible for the emitted luminosity. The luminosity is calculated by integrating this stress component over a radius within [5, 20] gravitational radii.

Although in a non-complicated approach, this work aims to advance the study in this area by using a fractional process as a perturbation, superimposed on a magnetized medium. As it is shown in the body of the paper (Section 3.4), an equilibrium deterministic magnetic field acquires a stochastic component following such a perturbation.

In the conclusions (Section 5), we review the signature of the input fBM on the output luminosity and its connections to observed LCs.

2 DISC CONFIGURATION AND EQUILIBRIUM

The initial configuration consists of a geometrically thin, optically thick rotating magnetized disc. By assumption the disc is non-viscous. The fundamental equations for accretion disc structure

★E-mail: gabriela.mocanu@ubbcluj.ro (GM); alexandru.marcu@phys.ubbcluj.ro (AM)

(e.g. equation set 6 from Balbus & Hawley 1998) are the continuity equation

$$\frac{\partial \rho}{\partial t} + \nabla \cdot (\rho \boldsymbol{v}) = 0, \tag{1}$$

the equation of motion for a magnetized plasma element

$$\rho \frac{\partial \boldsymbol{v}}{\partial t} + (\rho \boldsymbol{v} \cdot \nabla)\, \boldsymbol{v} = -\nabla P - \rho \nabla \phi_{\rm g} + \frac{1}{\mu_0} (\nabla \times \boldsymbol{B}) \times \boldsymbol{B}, \tag{2}$$

the induction equation

$$\frac{\partial \boldsymbol{B}}{\partial t} = \nabla \times (\boldsymbol{v} \times \boldsymbol{B}) \tag{3}$$

and the zero-divergence condition imposed on the magnetic field

$$\nabla \cdot \boldsymbol{B} = 0, \tag{4}$$

where ρ is the volume density, $\boldsymbol{v}$ is the velocity of the plasma element, P is the hydrostatic pressure in the disc, $\phi_{\rm g}$ is the gravitational potential due to the central source and $\boldsymbol{B}$ is the magnetic field permeating the disc.

Also, we use the assumption that the plasma in the disc is an ideal gas in the sense that the equation

$$p = \frac{k_{\rm B}}{\tilde{\mu} m_{\rm p}} \rho T \tag{5}$$

is valid, where $k_{\rm B}$ is the Boltzmann constant, $\tilde{\mu}$ is the mean molecular weight, $m_{\rm p}$ is the proton mass and T is the temperature.

The equilibrium disc is well described by a time-steady cylindrical symmetry (r, ϕ, z), such that $\partial/\partial t = \partial/\partial \phi = 0$. The disc structure may be characterized by a central temperature depending only on r and the dependence on the z coordinate may be neglected (Shakura & Sunyaev 1973). As a feature of the standard thin disc assumption, all the quantities should be considered as averages over height.

The gravitational potential outside the event horizon of the supermassive black hole is described by the Newtonian potential $\phi_{\rm g}(r) = -\frac{GM}{r}$, where G is the gravitational constant and M is the mass of the black hole. A test plasma volume in a Keplerian disc experiences a velocity equal to the Kepler velocity $\boldsymbol{v}_0(r) = (0, u_k(r), 0)\,; u_k(r) = \sqrt{GM/r}$, and an angular velocity equal to the Kepler angular velocity $\boldsymbol{\Omega}_0(r) = (0, 0, \Omega_k(r))\,; \Omega_k(r) = \sqrt{GM/r^3}$.

The equilibrium magnetic field is set up to have a zero radial component. Observations place the value of the magnetic field in the disc around the modest value of $\approx 10^{-8\pm1}$T (Kellerman & Pauliny-Toth 1969).

The numerical values chosen for the boundary parameters do not necessarily satisfy the zero-torque boundary condition on the inner orbit. Historically, the stress on the most inner orbit of the disc was considered to be zero but recent discussions on this topic have led to the conclusion that this assumption must be relaxed. For example, in recent work, Agol & Krolik (2000) numerically investigate a disc by taking into account general relativistic effects, non-zero torque at the boundary and find that the radiation returning from the inner area (which was previously decoupled from the disc because of the no-torque boundary condition) causes various annuli in the disc to 'communicate' on the light crossing time-scale. Communication on this time-scale is a feature needed by any model trying to explain IDV, because observational data show that if the source of IDV is in the disc, it needs to propagate on these time-scales (Dexter & Agol 2011; Mocanu & Sándor 2012).

Similar to the standard disc model (Shakura & Sunyaev 1973, 1976), the height-averaged equilibrium density as $\rho_0(r) \sim r^{-\theta}$ with $\theta = 15/8$ and the equilibrium temperature is taken as $T_0(r) = kr^{-\tau}$. This is justified based on the self-similarity property of the disc solutions (Blandford & Payne 1982) and on a set of observations. For example, the optical/UV continuum of NGC 7469 corresponds with the prediction for a $T_{\rm eff} \sim r^{-3/4}$ (Koratkar & Blaes 1999). Gaskell (2008) reports on a set of observations where the observed optical–UV spectral energy distribution implies a temperature $T \sim r^{-0.57}$, independent of the thickness of the disc. Simple blackbody disc models around supermassive black holes have $T_{\rm max}$ less than $3-8 \times 10^5$K and the UV and optical continuum emitting region is placed in the region between 10 and $100 r_{\rm g}$ (Balbus & Hawley 1998; Koratkar & Blaes 1999), where $r_{\rm g}$ is the gravitational radius $r_{\rm g} = 2GM/c^2$. For a central mass of $M = 10^8\,{\rm M}_\odot$, the accretion flow region responsible for the observed optical/UV spectrum is $\approx 10 r_{\rm g}$ (Koratkar & Blaes 1999) and $T \approx 10^5$ K is a characteristic temperature within about $30 r_{\rm g}$ (Frank, King & Raine 2002).

Based on these arguments, the numerical values of the parameters used throughout this analysis (all expressed in SI units) are:

(i) physical constants

$$\tilde{\mu} = 1.27,\ c = 3 \times 10^8,\ {\rm M}_\odot = 2 \times 10^{30},\ G = 6.6 \times 10^{-11},$$
$$k_{\rm B} = 1.3 \times 10^{-23},\ \mu_0 = 4\pi 10^{-7},\ m_{\rm p} = 1.6 \times 10^{-27}, \tag{6}$$

(ii) model assumptions

$$\tau = -3/4,\ M = 10^8\,{\rm M}_\odot,\ r_{\rm o} = 20 r_{\rm g},\ r_{\rm i} = 5 r_{\rm g},$$
$$\theta = 15/8,\ k = 2.6510^{14}. \tag{7}$$

where $r_{\rm o}$ and $r_{\rm i}$ are the outer and inner radii of the section of the disc considered to produce the optical radiation.

3 DENSITY PERTURBATION

The equilibrium state is perturbed by a prescribed temporal variation in the density. When the perturbation is applied, the new physical parameters that satisfy the MHD equations consist of a sum of two parts: the equilibrium part and the perturbed part.

The perturbations are isothermal. This is not because we believe that this is necessarily the case in an astrophysical disc. We make this assumption because in this toy model we want to study fluctuations in energy occurring at the same temperature, and not the distribution of energy in a large interval of temperatures.

Accretion is possible due to the outward angular momentum transport by a sum of Reynolds and Maxwell stresses (Balbus & Hawley 1991, 1998; Blaes 2002), and we assume that the perturbations in this mechanism are responsible for the variability. The component of the stress tensor responsible for the luminosity is defined as

$$m_{r\phi}(r,t) = \mu_0 \rho_0(r) v_r(r,t) v_\phi(r,t) - B_r(r,t) B_\phi(r,t), \tag{8}$$

where v_r, v_ϕ, b_r, b_ϕ are the perturbed components of the velocity and magnetic field.

The luminosity emitted from a patch of the disc due to the perturbation, between radii r_1 and r_2 is (Blaes 2002)

$$L_{12}(t) = \int_{r_1}^{r_2} m_{r\phi}(r,t) {\rm d}r \tag{9}$$

and this equation is the starting point of producing the LCs shown in the results section of the paper.

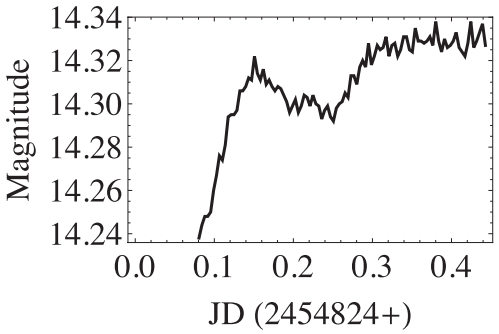

Figure 1. B (blue) band time series for the object BL Lacertae S5 0716+714; JD stands for Julian Day.

3.1 Stochastic density perturbation

There is a general consensus that the underlying mechanism producing IDV is stochastic (Lyubarskii 1997; Arevalo, McHardy & Summons 2008; MacLeod et al. 2010).

The time dependence of the density perturbation is taken to be the realization of a stochastic process such that $\frac{\partial \rho_1}{\partial t} = A_\rho B_H(t) = \xi$, where $B_H(t)$ is a normalized fBM and A_ρ is a constant amplitude, which will be prescribed by us. It is expected that locally fluctuating component of magnetic field create numerous current sheets inside the disc (Machida, Hayashi & Matsumoto 2000), which can be used as random reconnection sites. The accretion disc can work as a dynamo amplifying the stochastic magnetic field (Beskin 2010). This happens because even in a perfectly conducting plasma, turbulence develops through the magnetorotational instability (Spruit 2014). The already mentioned peculiar shape of the observational PSD prompts us to consider that the perturbation is a signal with non-Markovian properties. A sample LC is shown in Fig. 1.

There is no constraint imposed to the value of H in our framework mainly because there is a lack of observational data to correlate IDV characteristics to characteristics of the central engine. For example, Nesci, Massaro & Montagni (2002) report, regarding the optical IDV of S5 0716+714, that there is no correlation between the source magnitude and the amplitude of the IDV and that there is no clear correlation between the source magnitude and the rate of magnitude variation; Wagner & Witzel (1995) report that time-scales of optical variability in BL Lacs do not correlate with luminosity; MacLeod et al. (2010) conclude that it cannot be assumed that quasars with similar mass will necessarily have the same variability properties; Heidt & Wagner (1995) discuss optical data of a sample of BL Lac and state that there are no dependences of the time-scales on intrinsic properties, redshift or absolute magnitude.

The *definition* of fBM is (Mandelbrot & Van Ness 1968)

$$B_H(t) = \frac{1}{\Gamma\left(H+\frac{1}{2}\right)}\left(\int_{-\infty}^{0}\left[(t-s)^{H-1/2}-(-s)^{H-1/2}\right]\mathrm{d}B(s)\right) + \frac{1}{\Gamma\left(H+\frac{1}{2}\right)}\left(\int_{0}^{t}(t-s)^{H-1/2}\mathrm{d}B(s)\right), \quad (10)$$

where Γ represents the special function

$$\Gamma(z) = \int_0^\infty x^{z-1}\mathrm{e}^{-x}\mathrm{d}x. \quad (11)$$

The PSD of such a signal depends on the Hurst parameter H as (Mandelbrot & Van Ness 1968)

$$P(f) \sim f^{1-2H}. \quad (12)$$

If time is discretized as $t = hk$, with h a constant timestep, the sequence of increments

$$G_H(k) = B_H(k) - B_H(k-1) \quad (13)$$

is what is sometimes called fractional Gaussian noise, with the property that it is causally strongly connected with itself even at infinite temporal range. This is seen by calculating the expectation value of the correlation function of this signal in the limit of an infinite numbers of timesteps

$$\lim_{k\to\infty} E\left[G_H(j)G_h(j+k)\right] \sim H(2H-1)k^{2H-2} \neq 0 \quad (14)$$

for $H \notin \{0, 1/2\}$. So stated more clearly, the number H is an indication of the memory of the process: the fBM B_H has increments that are not independent of each other.

The set $\{v_r, v_\phi, B_r, B_\phi\}$ at each position and timestep is needed. The necessary MHD equations are written as stochastic differential equations, with $\xi(t)$ as a source term.

3.2 Equations valid for general $\boldsymbol{B_0(r) = \{0, B_\phi(r), B_z(r)\}}$

After linearizing the perturbed set of MHD equations and selecting just the needed set of variables, it is obtained that

$$\frac{\partial \rho_1}{\partial t} + \frac{\rho_0}{r}\frac{\partial (r v_\mathrm{r})}{\partial r} + v_\mathrm{r}\frac{\mathrm{d}\rho_0}{\mathrm{d}r} = 0, \quad (15)$$

$$\frac{\partial v_\phi}{\partial t} + v_\mathrm{r}\left(\frac{u_k}{r} + \frac{\mathrm{d}u_k}{\mathrm{d}r}\right) = \frac{1}{\mu_0\rho_0}\frac{a_1}{r^2}\frac{\mathrm{d}(r B_\phi)}{\mathrm{d}r}, \quad (16)$$

$$\frac{\partial b_\phi}{\partial t} = a_1\frac{\mathrm{d}(u_k/r)}{\mathrm{d}r} - \frac{\partial (v_\mathrm{r} B_\phi)}{\partial r}, \quad (17)$$

$$b_\mathrm{r} = \frac{a_1}{r}. \quad (18)$$

The continuity equation provides v_r in terms of $\xi(t)$

$$\rho_0(r)\frac{\partial v_\mathrm{r}(r,t)}{\partial r} + \left[\frac{\rho_0(r)}{r} + \frac{\mathrm{d}\rho_0(r)}{\mathrm{d}r}\right] = -\xi(t), \quad (19)$$

which when solved for the r variation with $v_\mathrm{r}(r_\mathrm{o}, t) = 0$ gives

$$v_\mathrm{r}(r,t) = \frac{r^{7/8}\left(-r^2 + r_\mathrm{o}^2\right)}{2a_2}\xi(t). \quad (20)$$

3.3 Configuration I of initial magnetic field

We study how a disc with a particular initial configuration will evolve when subjected to a stochastic density perturbation. We let $B_\phi = 0$ and

$$B_z(r) = \frac{b_0}{r}\sin\left[\frac{2\pi(r-r_\mathrm{i})}{r_\mathrm{o}-r_\mathrm{i}}\right]. \quad (21)$$

The value of b_0 is calculated by fixing the plasma beta $\beta = 2p_0\mu_0/B_0^2$ to a numerical value.

The ϕ component for the equation of motion and induction simplify and become

$$\frac{\partial v_\phi}{\partial t} + v_\mathrm{r}\left(\frac{u_k}{r} + \frac{\mathrm{d}u_k}{\mathrm{d}r}\right) = 0, \quad (22)$$

and

$$\frac{\partial b_\phi}{\partial t} = a_1\frac{\mathrm{d}(u_k/r)}{\mathrm{d}r}. \quad (23)$$

The solution for the magnetic field is, with $b_\phi(r, t = 0) = 0$

$$b_\phi(r, t) = -\frac{3a_1}{2}\frac{u_k}{r^2}t = -\frac{3a_1}{2}\Omega_0 t. \quad (24)$$

For this case, we find that the perturbed magnetic field is not a stochastic variable.

The equation for the azimuthal velocity becomes

$$\frac{\partial v_\phi}{\partial t} + \frac{1}{4a_2}u_k r^{-1/8}\left(-r^2 + r_o^2\right)A_\rho B_H(t) = 0. \quad (25)$$

The stochastic quantities in this configuration are v_r and v_ϕ and have defining equations

$$v_r(r, t) = f_1(r)B_H(t), \quad (26)$$

$$\frac{\partial v_\phi(r, t)}{\partial t} = f_2(r)B_H(t), \quad (27)$$

with

$$f_1(r) = A_\rho\frac{r^{7/8}\left(-r^2 + r_o^2\right)}{2a_2} \quad (28)$$

and

$$f_2(r) = -\frac{A_\rho}{4a_2}u_k r^{-1/8}\left(-r^2 + r_o^2\right). \quad (29)$$

We take advantage that there is no differential operator in r and write the defining equations in update form for the temporal variation

$$v_\phi(r, t + h) = v_\phi(r, t) + f_2(r)\sqrt{h}G_H(t) \quad (30)$$

with $v_\phi(r, 0) = 0$.

The way that a_1 is assigned a numerical value in this case takes advantage of the fact that $b_\phi(r, t = 0) = 0$, and that $b_r = a_1/r$ such that we start the simulation by imposing that at $t = 0$, the perturbed quantities have the same plasma beta as the equilibrium.

3.4 Configuration II of initial magnetic field

The shape of $B_z(r)$ is kept and $B_\phi(r) = \frac{b_0}{r}\cos[\frac{2\pi(r-r_i)}{r_o-r_i}]$. b_0 is again calculated based on plasma beta considerations.

In this case, the evolution equations for v_ϕ and b_ϕ are

$$v_\phi(r, t + h) = v_\phi(r, t) - f_3(r)h + f_4(r)\sqrt{h}G_H(t), \quad (31)$$

$$b_\phi(r, t + h) = b_\phi(r, t) + f_5(r)h - f_6(r)\sqrt{h}G_H(t), \quad (32)$$

where

$$f_3(r) = -\frac{1}{\mu_0\rho_0(r)}\frac{a_1}{r^2}\frac{\mathrm{d}(rB_\phi(r))}{\mathrm{d}r}, \quad (33)$$

$$f_4(r) = -\left(\frac{u_k}{r} + \frac{\mathrm{d}u_k}{\mathrm{d}r}\right)f_1(r), \quad (34)$$

$$f_5(r) = a_1\frac{\mathrm{d}u_k/r}{\mathrm{d}r}, \quad (35)$$

$$f_6(r) = \frac{\mathrm{d}B_\phi f_1}{\mathrm{d}r}. \quad (36)$$

With the assumptions of the model, it is clear from equation (32) that if there is a non-zero initial azimuthal magnetic field, the perturbed magnetic field will be a stochastic process.

4 RESULTS

The equations are implemented and solved in MATHEMATICA[1]. The numerical values for the luminosity are not expected to fit the observed ones. The graphical representation is done by dividing the values in the luminosity vector to its minimum value: one can than see by how much the luminosity increases in a time interval of 30 min. Variations on this time-scale have been reported for this object by, e.g., Wu (2005).

The simulation was carried for both initial magnetic field configurations (Sections 3.3 and 3.4). The set of variable parameters is $\{\beta, H\}$, the plasma beta characterizing the system and the Hurst parameter, characterizing the perturbation. We chose to let β take values $\in \{100, 1000\}$ and $H \in [0.1, 0.9]$ in increments of 0.1. If the disc would not modify the properties of the input perturbation it would be expected that the spectral slope would be the one given by equation (12), i.e. within an interval $(-1, 1)$ for $H \in (0, 1)$.

Conversely, if we assume that the spectral slope of the observed LCs is in a bijective relation with the Hurst parameter of the input perturbation, then this perturbation would have $H_0 \in (0.8, 1.6)$.

The main results of this work are the LCs produced by varying $\{\beta, H\}$ (a sample of such LCs is shown here in Figs 2 and 3) and most importantly the PSDs of these LCs, all displayed in Tables 1–12. A sample fit of the PSD is shown in Fig. 4, where the blue line is the best fit and the red line is the fit according to the polynomial assumption. Analysis of IDV observational data for this object place the value of the spectral slope α in a wide interval, ranging from 0.37 to 2.7 (see, e.g. table 2 from Mocanu & Marcu 2012).

All data vectors were checked for convergence (even though the trend in some figures seems to be increasing), but for consistency of the presentation only the first 30 min of all LCs are shown (one timestep equals one second). Observations show that optical LCs from BL Lac S5 0716+714 although variable are not periodic, e.g. Wagner & Witzel (1995) reports that optical observations never have constant duty-cycle; also, Chandra et al. (2011) found no periodicity during an observational campaign in 2009 March.

The tables were populated by using the R software (Vaughan 2010) according to the assumption that the emission process behaves so as to produce a luminosity with PSD $\sim f^{-\alpha}$. We impose this restriction because, as already discussed, many sets of observational data exhibit this behaviour. The second column in each table contains the value of the spectral slope α and the first column contains the Hurst parameter of the fBM perturbing the disc in that case. The errors associated with each α stem from the fact that the slope is calculated with the R software; essentially, these errors come from mediating over many realizations of a process with the same characteristics. The third column contains the Bayesian probability which assesses the correctness of the assumption, i.e. if p_B is close to 1, than the assumption is correct. For details about the technical procedure, see Vaughan (2010).

We would consider our model to be at least moderately successful if it would reproduce non-trivial values for α with high values of the Bayesian probability. A careful analysis of Tables 1–12 shows that this is indeed the case; a bold type letter was used to mark the most promising results.

There is one subtle issue that still needs to be discussed, namely what happens to the radiation after the local emission. The mathematics used so far assumed, according to the standard model, that the

[1] We acknowledge using the package (http://demonstrations.wolfram.com/OneDimensionalFractionalBrownianMotion) to draw numbers distributed according to an fBM process.

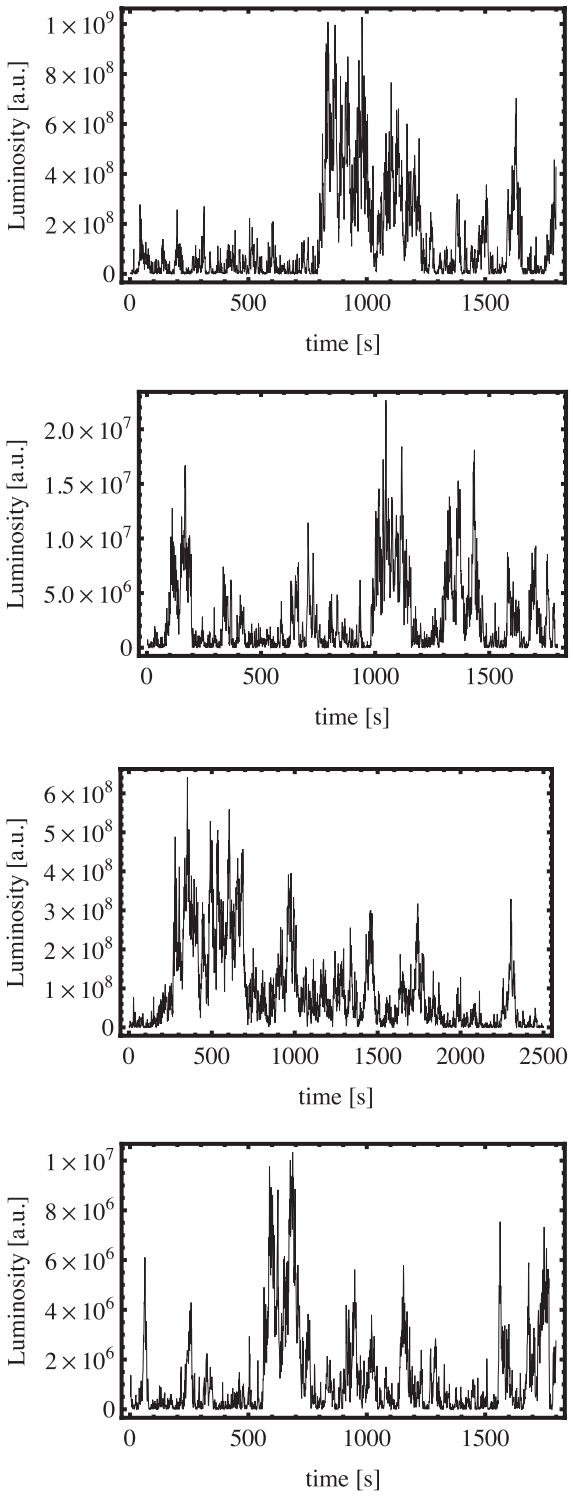

Figure 2. Simulated LCs for $H = 0.3$, $A_\rho = 10^{-3}$ and, from top to bottom, configuration I $\beta = 100$ and 1000, configuration II $\beta = 100$ and 1000.

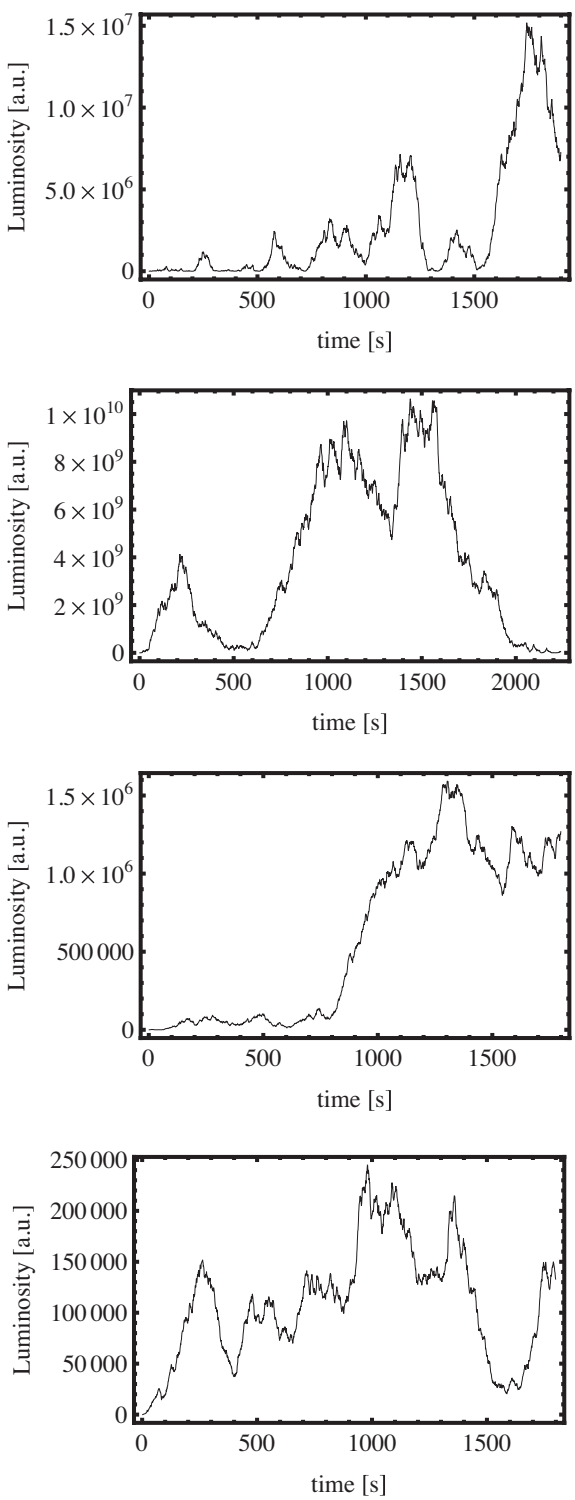

Figure 3. Simulated LCs for $H = 0.7$, $A_\rho = 10^{-3}$ and, from top to bottom, configuration I $\beta = 100$ and 1000, configuration II $\beta = 100$ and 1000.

produced radiation comes from a height-averaged quantity; let us call this the 'observed' radiation. However, from its production spot in the disc and before leaving the body of the disc, the local radiation goes through diffusion in the thickness (albeit small) of the disc. So the local radiation, upon diffusion, becomes the observed radiation. There would appear to be an inconsistency in our treatment: we use tools to obtain the observed radiation (height-averaged equations) but use local perturbation (the fBM). This apparent inconsistency can be dealt with by providing an answer to the question: Are statistical properties of the distribution of isothermal photons (which are responsible for the local radiation) changed if they are subjected to unbiased random walk (diffusion through the body of the disc)? Recall that our aim is to offer a possible explanation of the PSD of the observed LCs. Since unbiased random walk through a medium

Table 1. PSD of the output curve for a range of Hurst parameters of the input signal, for configuration I, $\beta = 100$, $r \in [5r_g, 20r_g]$.

H	α	p_B
0.1	0.6111 [±0.03]	0.888
0.2	1.1243 [±0.03]	0.688
0.3	1.1298 [±0.03]	0.432
0.4	1.5573 [±0.03]	0.604
0.5	1.8014 [±0.032]	0.842
0.6	1.994 [±0.033]	0.203
0.7	1.973 692 [±0.027]	0.266
0.8	1.8706 [±0.029]	0.147
0.9	1.8113 [±0.03]	1.0

Table 2. PSD of the output curve for a range of Hurst parameters of the input signal, for configuration II, $\beta = 100$, $r \in [5r_g, 20r_g]$.

H	α	p_B
0.1	0.4782 [±0.030]	0.837
0.2	1.1112 [±0.029]	0.455
0.3	1.326 146 [±0.025]	0.196
0.4	1.5925 [±0.031]	0.192
0.5	1.7372 [±0.031]	0.41
0.6	1.915 [±0.03]	0.459
0.7	1.8411 [±0.029]	0.995
0.8	2.5653 [±0.031]	0.835
0.9	1.8059 [±0.028]	0.998

Table 3. PSD of the output curve for a range of Hurst parameters of the input signal, for configuration I, $\beta = 1000$, $r \in [5r_g, 20r_g]$.

H	α	p_B
0.1	0.6786 [±0.026]	0.171
0.2	0.9013 [±0.03]	0.131
0.3	1.2751 [±0.033]	0.796
0.4	1.5198 [±0.031]	0.134
0.5	1.7639 [±0.031]	0.402
0.6	1.8806 [±0.032]	1.0
0.7	2.250 149 [±0.028]	0.74
0.8	1.8333 [±0.031]	1.0
0.9	1.9412 [±0.026]	0.015

Table 4. PSD of the output curve for a range of Hurst parameters of the input signal, for configuration II, $\beta = 1000$, $r \in [5r_g, 20r_g]$.

H	α	p_B
0.1	0.7734 [±0.029]	0.329
0.2	0.8547 [±0.031]	0.083
0.3	1.2811 [±0.029]	0.255
0.4	1.6303 [±0.029]	0.102
0.5	1.771 [±0.03]	0.12
0.6	1.875 [±0.028]	1.0
0.7	2.0087 [±0.029]	0.757
0.8	1.8255 [±0.029]	1.0
0.9	2.1951 [±0.026]	0.001

Table 5. PSD of the output curve for a range of Hurst parameters of the input signal, for configuration I, $\beta = 100$, $r \in [5r_g, 50r_g]$.

H	α	p_B
0.1	0.699 [±0.02]	0.022
0.2	1.0 [±0.02]	0.486
0.3	1.332 [±0.01]	0.525
0.4	1.605 [±0.02]	0.09
0.5	1.806 [±0.02]	0.368
0.6	2.016 [±0.02]	0.341
0.7	1.901 [±0.02]	0.506
0.8	1.862 [±0.02]	0.1
0.9	2.692 [±0.02]	0.774

Table 6. PSD of the output curve for a range of Hurst parameters of the input signal, for configuration I, $\beta = 1000$, $r \in [5r_g, 50r_g]$.

H	α	p_B
0.1	0.752 [±0.01]	0.218
0.2	0.936 [±0.02]	0.311
0.3	1.360 [±0.02]	0.971
0.4	1.672 [±0.02]	0.967
0.5	1.822 [±0.02]	0.962
0.6	1.928 [±0.02]	0.794
0.7	1.988 [±0.01]	0.529
0.8	1.835 [±0.02]	0.655
0.9	1.977 [±0.01]	0.004

Table 7. PSD of the output curve for a range of Hurst parameters of the input signal, for configuration II, $\beta = 100$, $r \in [5r_g, 50r_g]$.

H	α	p_B
0.1	0.697 [±0.02]	0.036
0.2	1.017 [±0.02]	0.779
0.3	1.414 [±0.02]	0.136
0.4	1.551 [±0.02]	0.227
0.5	1.795 [±0.02]	0.722
0.6	1.866 [±0.02]	1.0
0.7	2.244 [±0.01]	0.002
0.8	1.812 [±0.02]	1.0
0.9	1.798 [±0.01]	1.0

Table 8. PSD of the output curve for a range of Hurst parameters of the input signal, for configuration II, $\beta = 1000$, $r \in [5r_g, 50r_g]$.

H	α	p_B
0.1	0.611 [±0.02]	0.637
0.2	1.009 [±0.02]	0.061
0.3	1.404 [±0.02]	0.477
0.4	1.581 [±0.02]	0.333
0.5	1.830 [±0.02]	0.806
0.6	1.853 [±0.02]	1.0
0.7	2.255 [±0.02]	0.665
0.8	1.981 [±0.02]	0.532
0.9	2.189 [±0.02]	0.37

Table 9. PSD of the output curve for a range of Hurst parameters of the input signal, for configuration I, $\beta = 100$, $r \in [5r_g, 100r_g]$.

H	α	p_B
0.1	0.720 [±0.02]	0.082
0.2	0.953 [±0.02]	0.015
0.3	1.336 [±0.01]	0.391
0.4	1.567 [±0.02]	0.136
0.5	1.801 [±0.02]	0.039
0.6	2.011 [±0.02]	0.751
0.7	1.873 [±0.02]	1.0
0.8	1.857 [±0.02]	1.0
0.9	1.810 [±0.02]	1.0

Table 10. PSD of the output curve for a range of Hurst parameters of the input signal, for configuration I, $\beta = 1000$, $r \in [5r_g, 100r_g]$.

H	α	p_B
0.1	0.733 [±0.02]	0.042
0.2	1.089 [±0.02]	0.465
0.3	1.417 [±0.02]	0.335
0.4	1.606 [±0.02]	0.215
0.5	1.851 [±0.02]	0.036
0.6	1.836 [±0.02]	1.0
0.7	2.010 [±0.02]	0.401
0.8	1.828 [±0.02]	1.0
0.9	1.828 [±0.02]	1.0

Table 11. PSD of the output curve for a range of Hurst parameters of the input signal, for configuration II, $\beta = 100$, $r \in [5r_g, 100r_g]$.

H	α	p_B
0.1	0.685 [±0.02]	0.096
0.2	0.998 [±0.02]	0.954
0.3	1.365 [±0.02]	0.55
0.4	1.642 [±0.02]	0.427
0.5	1.746 [±0.02]	0.754
0.6	2.033 [±0.02]	0.692
0.7	1.936 [±0.02]	0.973
0.8	1.907 [±0.02]	0.629
0.9	1.825 [±0.02]	1.0

Table 12. PSD of the output curve for a range of Hurst parameters of the input signal, for configuration II, $\beta = 1000$, $r \in [5r_g, 100r_g]$.

H	α	p_B
0.1	0.693 [±0.02]	0.041
0.2	1.067 [±0.02]	0.042
0.3	1.399 [±0.02]	0.37
0.4	1.531 [±0.02]	0.977
0.5	1.845 [±0.02]	0.02
0.6	2.018 [±0.02]	0.849
0.7	1.843 [±0.02]	1.0
0.8	1.827 [±0.02]	1.0
0.9	1.883 [±0.02]	0.11

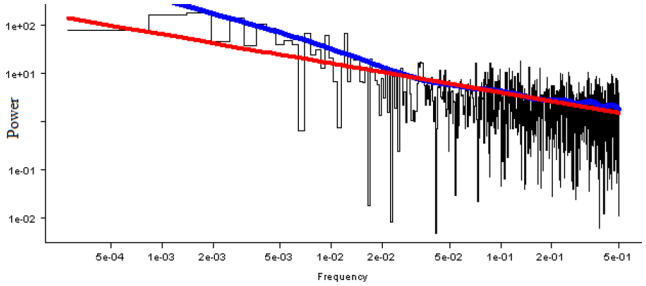

Figure 4. Sample PSD output of Bayes R for configuration I, $H = 0.1$, $A_\rho = 10^{-3}$ and $\beta = 100$.

cannot influence temporal correlation of otherwise identical (same temperature) photons, we will use the term 'observed' radiation for our results.

Comparison with the statistical properties of observational data for a BL Lac, e.g. analysed in Mocanu & Marcu (2012), is good.

Regarding the connection between α and H in the space parameter of the two different configurations, the plasma β and different radial extents of the simulated disc, we produced plots $\alpha(H)$ with varying radial extent (Figs 5–8). It does not seem that extending the disc produces significant changes in the shape of the relationship. As expected, the dependence is not linear. In fact, it can be seen from the plots that $\alpha(H)$ reaches a plateau, with a different value for each

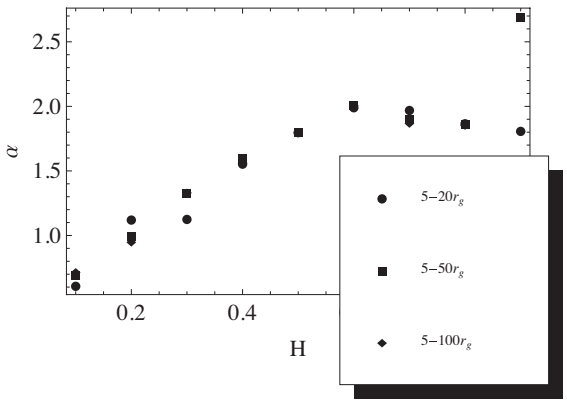

Figure 5. A plot of the output spectral slope α as a function of the input Hurst parameter $H \in \{0.1, 0.9\}$ for configuration I, $\beta = 100$ and various radial extents of the disc.

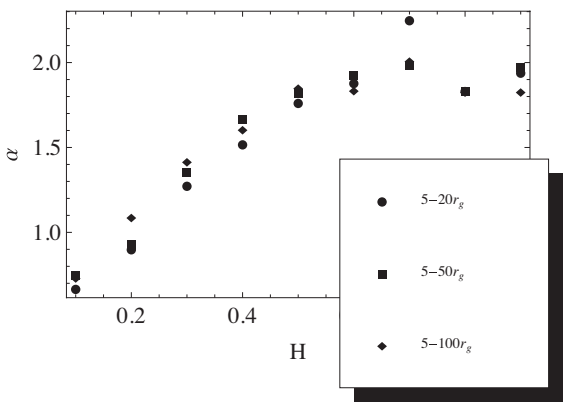

Figure 6. A plot of the output spectral slope α as a function of the input Hurst parameter $H \in \{0.1, 0.9\}$ for configuration I, $\beta = 1000$ and various radial extents of the disc.

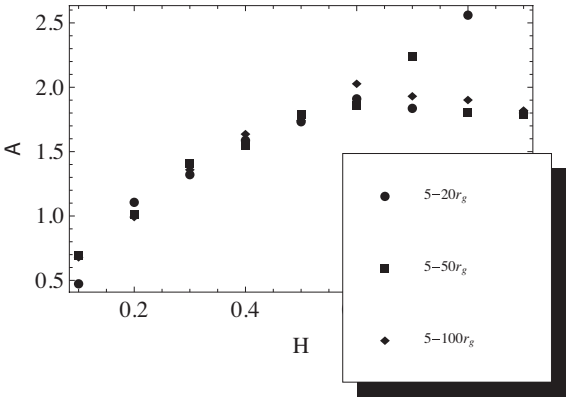

Figure 7. A plot of the output spectral slope α as a function of the input Hurst parameter $H \in \{0.1, 0.9\}$ for configuration II, $\beta = 100$ and various radial extents of the disc.

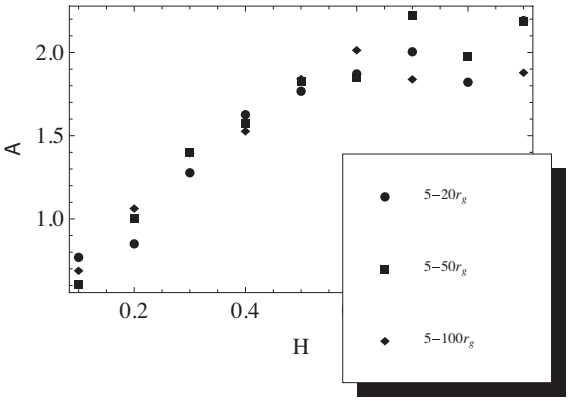

Figure 8. A plot of the output spectral slope α as a function of the input Hurst parameter $H \in \{0.1, 0.9\}$ for configuration II, $\beta = 1000$ and various radial extents of the disc.

of the configurations considered. However, these results should be taken with caution as the points in the plots do not all have equal Bayesian probability (the p_B from the tables is different).

5 CONCLUSIONS

The appearance of a perturbed magnetized accretion disc was investigated for the realistic case of a stochastic density perturbation and the output was investigated as a function of the Hurst parameter of the input signal. Two possible configurations of an initial magnetic field were considered. The most important result is the set of values obtained for the spectral slope and the corresponding Bayesian probabilities (α and p_B, shown in Tables 1–12). The simulated curves are found to reproduce the PSD characteristics of observed IDV data.

Although left with important things to fine-tune, this toy model may turn out to be very useful in explaining IDV. Future research in this area would benefit from focusing on finding a physics-based analytical bijective relation between input perturbation and produced LCs.

ACKNOWLEDGEMENTS

The authors thank the referee for valuable comments and suggestions, which increased the quality and overall accuracy of this paper. This work was supported by a grant of the Romanian National Authority of Scientific Research, Program for research – Space Technology and Advanced Research – STAR, project number 72/29.11.2013.

REFERENCES

Agol E., Krolik J. H., 2000, ApJ, 528, 161
Arevalo P., McHardy I. M., Summons D. P., 2008, MNRAS, 388, 211
Azarnia G. M., Webb J. R., Pollock J. T., 2005, IAPPP Commun., 101, 1
Balbus S. A., Hawley J. F., 1991, ApJ, 376, 214
Balbus S. A., Hawley J. F., 1998, Rev. Mod. Phys., 70, 1
Beskin V. S., 2010, MHD Flows in Compact Astrophysical Objects. Accretion, Winds and Jets. Springer-Verlag, Berlin
Blaes O. M., 2002, in Beskin V., Henri G., Menard F., Pelletier G., Dalibard J., eds, Physics Fundamentals of Luminous Accretions Disks Around Black Holes. Springer-Verlag, Berlin, p. 139
Blandford R. D., Payne D. G., 1982, MNRAS, 199, 883
Carini M. T., Walters R., Hopper L., 2011, ApJ, 141, 49
Chanda S., Balyian K. S., Ganesh S., Joshi U. C., 2011, ApJ, 731, 118C
Dexter J., Agol E., 2011, ARA&A, 727, L24
Frank J., King A., Raine D., 2002, Global Accretion Power in Astrophysics, 3rd edn. Cambridge Univ. Press, New York
Gaskell C. M., 2008, Revista Mexicana de Astronomía y Astrofísica, 32, 1
Heidt J., Wagner S. J., 1995, A&A, 305, 45
Kellerman K. I., Pauliny-Toth I. I. K., 1969, ApJ, 155, 71
Koratkar A., Blaes O., 1999, PASP, 111, 1
Krichbaum T. P., Kraus A., Fuhrman L., Cimo G., Witzel A., 2002, Publ. Astron. Soc. Aust., 19, 14
Leung C. S., Wei J. Y., Harko T., Kovacs Z., 2011, J. Astrophys. Astron., 32, 189
Lyubarskii Y. E., 1997, MNRAS, 292, 679
Machida M., Hayashi M. R., Matsumoto R., 2000, ApJ, 532, L67
MacLeod C. L. et al., 2010, ApJ, 721, 1014
Mandelbrot B. B., Van Ness V., 1968, SIAM Rev., 10, 422
Mineshige S., Ouchi N. B., Nishimori H. T., 1994, PASJ, 46, 97
Mocanu G. R., Marcu A., 2012, Astron. Nachr., 333, 166
Mocanu G. R., Sándor B., 2012, ARA&A, 342, 147
Montagni F., Maselli A., Massaro E., Nesci R., Sclavi S., Maesano M., 2006, A&A, 451, 435
Nesci S., Massaro E., Montagni F., 2002, Publ. Astron. Soc. Aust., 19, 143
Poon H., Fan J. H., Fu J. N., 2009, ApJS, 185, 511
Shakura N. I., Sunyaev R. A., 1973, A&A, 24, 337
Shakura N. I., Sunyaev R. A., 1976, MNRAS, 175, 613
Spruit H. C., 2014, "Accretion disks", Accretion Processes in Astrophysics, 1st edn. Cambridge Univ. Press, Cambridge
Vaughan S., 2010, MNRAS, 402, 307
Wagner S., Witzel A., 1995, ARA&A, 33, 163
Wagner S. et al., 1996, AJ, 111, 2187
Wu J., Peng B., Zhou X., Ma J., Jiang Z., Chen J., 2005, AJ, 129, 1818

This paper has been typeset from a TEX/LATEX file prepared by the author.